Electronic Supplementary Material

Precursor-driven structural tailoring of iron oxychloride for enhanced heterogeneous Fenton activity

Shengshuo Xu[1], Zhenying Lu[1], Jinling Wang[1,2], Guangtuan Huang[1], Hualin Wang[1,2], Xuejing Yang (✉)[1,2]

1 National Engineering Laboratory for Industrial Wastewater Treatment, East China University of Science and Technology, Shanghai 200237, China

2 State Key Laboratory of Chemical Engineering, East China University of Science and Technology, Shanghai 200237, China

E-mail: xj.yang@ecust.edu.cn

1. SEM characterization

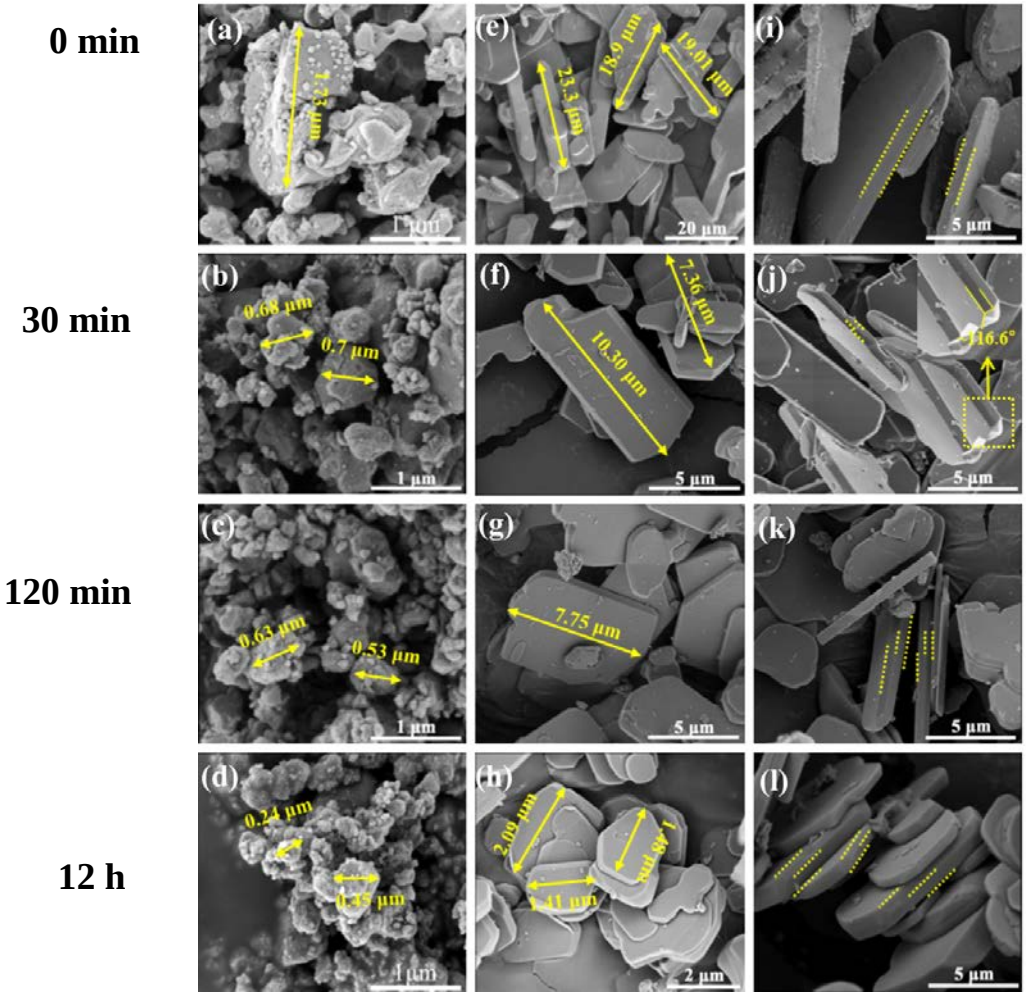

Fig. S1. The SEM images of the hematite precursors with different milling durations (a-d) and their derived FeOCl (e-l)

Since FeOCl adopts an orthorhombic structure, the formula for the angle of each crystal plane follows the formula eq. S1-eq. S2.

$$\cos\varphi = \frac{\frac{h_1h_2}{a^2}+\frac{k_1k_2}{b^2}+\frac{l_1l_2}{c^2}}{\sqrt{(\frac{h_1^2}{a}+\frac{k_1^2}{b}+\frac{l_1^2}{c})(\frac{h_2^2}{a}+\frac{k_2^2}{b}+\frac{l_2^2}{c})}} \qquad \text{eq. S1}$$

$$\cos\varphi = \frac{\frac{\pm1}{b^2}}{\sqrt{(\frac{1^2}{a}+\frac{1^2}{b})(\frac{1^2}{b})}} \qquad \text{eq. S2}$$

a, b, c are the unit cell parameters of FeOCl ;a=3.7802 Å ; b=7.917 Å;c=3.302 Å.[1]

It can be calculated that the angle between the (110/1-10) crystal plane and the

(010) crystal plane is 115°, which appears on the side of the (010) crystal plane. As seen in Fig. S1(i-l), the side of pristine FeOCl is smooth and contains no edges. Combined with the TEM results, the basal plane surface exposed on pristine FeOCl is (010), and its side should be (200) crystal plane. After the precursors ground for 30 minutes, the side planes appeared. The angle between the inclined face and the (010) surface is 116.6°, which is close to the theoretical value of 115°. Therefore, it was proposed that the inclined plane was attributed to the (110/1-10) crystal plane. As the particle size decreased, it could be observed that a similar phenomenon of the edge and oblique planes appeared on the side of FeOCl, which could be judged as high energy (110/1-10) crystal plane.

2. Infrared vibration of Fe-O

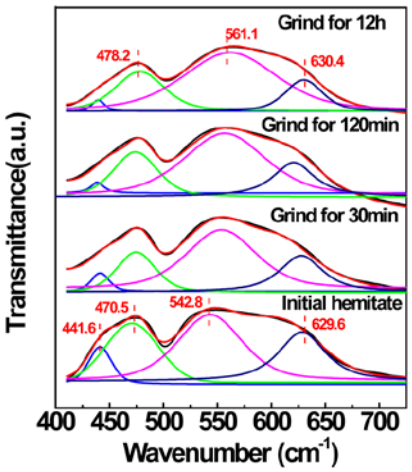

Fig. S2. Fitted vibration peaks of infrared Fe-O bonds with hematite precursors under grinding for different durations.

Table S1. The percentage of each IR peak area at different wavenumbers for hematite grinded under different grinding durations.

FTIR wavenumber	440 cm^{-1}	480 cm^{-1}	540 cm^{-1}	630 cm^{-1}
Initial Fe_2O_3	0.089	0.242	0.631	0.132
Fe_2O_3- Grind 30min	0.042	0.220	0.566	0.190
Fe_2O_3-Grind 120min	0.020	0.211	0.526	0.231
Fe_2O_3-Grind 12h	0.015	0.201	0.403	0.305

3. particle size and specific surface area of different FeOCl

Table S2. Characterization of particle size and specific surface area of different FeOCl.

Materials	LPSA(MV,μm)	SEM(μm)	BET(m^2/g)
FeOCl-P	10.48	3-15	8.93
FeOCl-30nm	6.47	3-9	/
FeOCl-0.5h	9.85	2-10	/
FeOCl-2h	7.8	2-7.8	/
FeOCl-12h	4.36	3	34.28

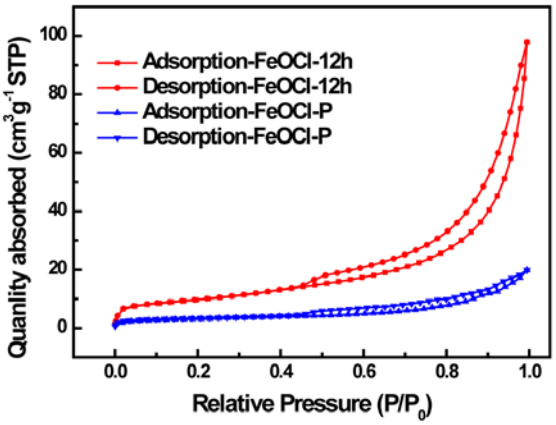

Fig. S3. The nitrogen isotherm adsorption-desorption curves of pristine FeOCl and FeOCl-12h.

4. The intensity diffraction peak ratio from XRD patterns

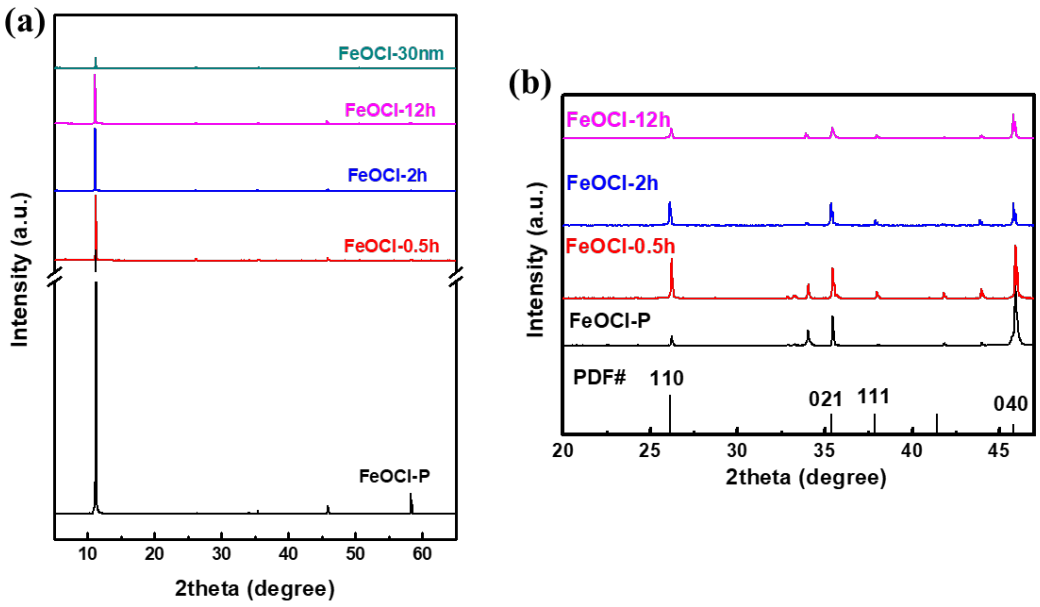

Fig. S4. (a) The XRD patterns of FeOCl synthesized from hematite subjected to different milling times. (b) The diffraction peaks of different FeOCl at high Bragg angles.

Table S3. Diffraction peak intensity ratio of hematite and FeOCl from corrected XRD

Intensity ratios from XRD		Initial Fe_2O_3	Fe_2O_3-30min	Fe_2O_3-120min	Fe_2O_3-12h
I (104):I (110)	Area	1.39	1.35	1.28	1.32
	Height	1.62	1.45	1.36	1.19

Intensity ratios from XRD		FeOCl-P	FeOCl-30nm	FeOCl-30min	FeOCl-120min	FeOCl-12h
I (010):I (110)	Area	500	66.67	21.74	11.63	6.29
	Height	500	37.04	25.64	12.82	7.30

Based on the corrected XRD pattern, the (110) and (010) intensity ratios for different FeOCl were calculated. The proportion of $I_{(110)}$ increases with the reduced sizes of FeOCl particles, which indicates that the growth orientation of small-sized FeOCl in the [110] direction was increasing. Combined with the SEM images in Fig. S1, the (110) crystal plane was gradually exposed to the surface as the FeOCl particle

size became smaller.

5. The adsorption capacity of the obtained FeOCl series materials

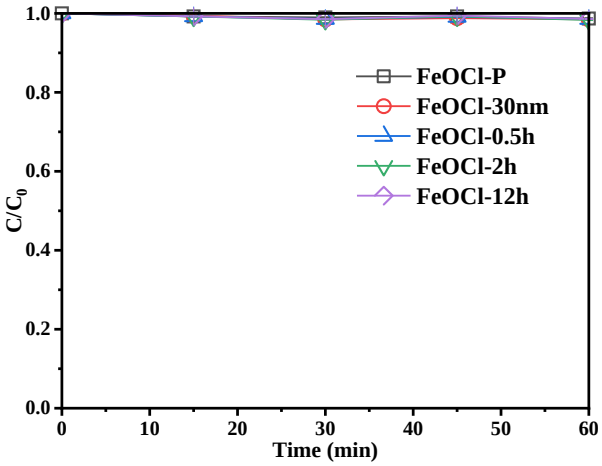

Fig. S5. Activity of different FeOCl for adsorption of phenol. Reaction conditions: Phenol concentration of 50 ppm; catalyst dosage of 500 ppm; pH=4.0 (4mM HAc-NaAc); 25℃.

6. EPR signal

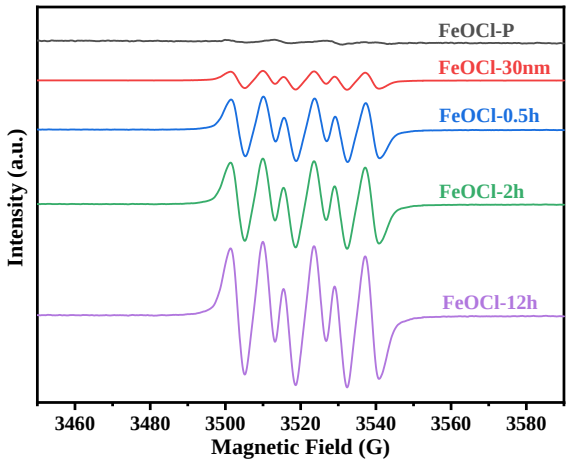

Fig. S6. EPR signals obtained in methanol containing 180 mM DMPO + 500 mg/L FeOCl + 30mM H_2O_2.

7. Surface energy calculation

Table S4. Surface energy calculation of (100), (110), (010) crystal planes

facet	E_{bulk}(eV)	$E_{slab}^{unrelax}$(eV)	E_{slab}^{relax}(eV)	A (Å^2)	n	γ (J/m^2)
100		-152.206	-152.68	26.163	5	0.0315522
110	-30.961	-152.191	-152.543	28.569	5	0.0334278
010		-154.74	-154.77	12.11		0.00012

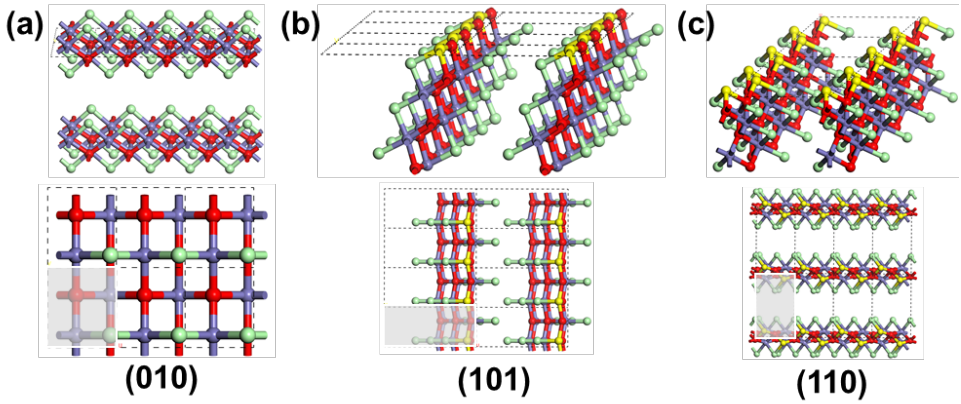

Fig. S7. Surface structures of crystal plane (a) (010) and (b) (110) of FeOCl Surface structure for evaluating adsorption energy. The dotted lines indicate the lattice surfaces.

8. The detailed XPS data of tailored FeOCl with different sizes.

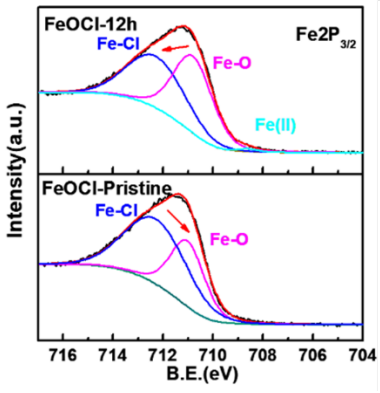

Fig. S8. XPS spectrum of Fe2p$_{3/2}$ from pristine FeOCl-P and FeOCl-12 h.

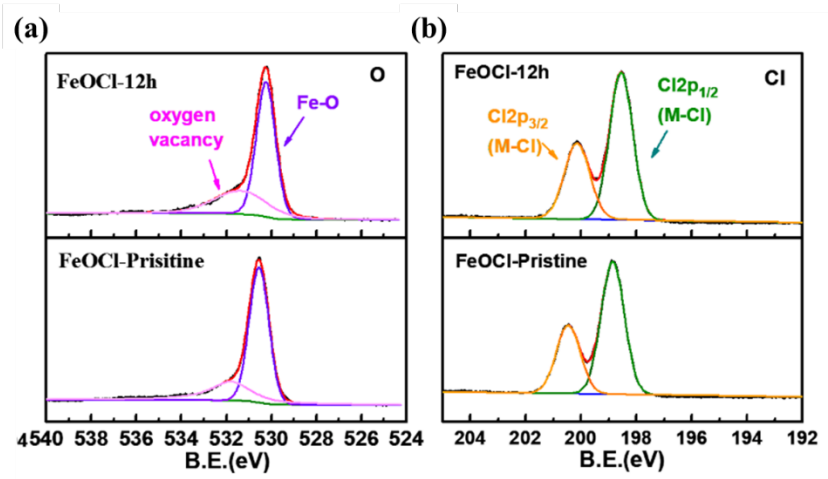

Fig. S9. XPS spectrum of (a) O1s and (b) Cl 2p from pristine FeOCl-P and FeOCl-12 h.

Table S5. Surface element content calculated by XPS and the peak-fitting result of Fe $2p_{3/2}$ spectra of each size FeOCl

Different FeOCl	**Atomic percentage of XPS (%)**		
	Fe	**Cl**	**O**
FeOCl-Pristine	6.25	8.09	10.88
FeOCl-0.5h	6.44	5.34	13.45
FeOCl-2h	6.50	5.19	13.57
FeOCl-12h	6.56	4.63	14.05

Catalysts		**B.E. (eV)**	**Area**	**Percentage**
FeOCl-Pristine	Fe(III)-O	711.0	22193.3	37.3%
	Fe(III)-Cl	712.3	37312.1	67.2%
	Fe(II)	708.52	1283	1.3%
FeOCl-0.5h	Fe(III)-O	710.9	29086.9	43.9%
	Fe(III)-Cl	712.3	36277.5	54.8%
	Fe(II)	708.6	1316	2.03%
FeOCl-2h	Fe(III)-O	710.8	30312.3	46.8%
	Fe(III)-Cl	712.3	33087.8	51.17%
	Fe(II)	708.6	1328	2.05%
FeOCl-12h	Fe(III)-O	710.8	33025	50.98%
	Fe(III)-Cl	712.2	30416	46.97%

9. Intermediate/product variation versus time and phenol degradation path

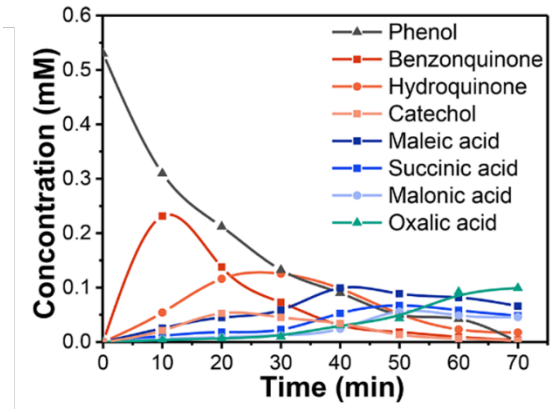

Fig. S10. Intermediate products detected in the phenol degradation process in this Fenton-like system. 50 ppm phenol + 500 ppm FeOCl-12h + 5.9 mg/L NaCl + 30 mM H_2O_2 (pH = 4, 4 mM HAc-NaAc buffer, 25 °C).

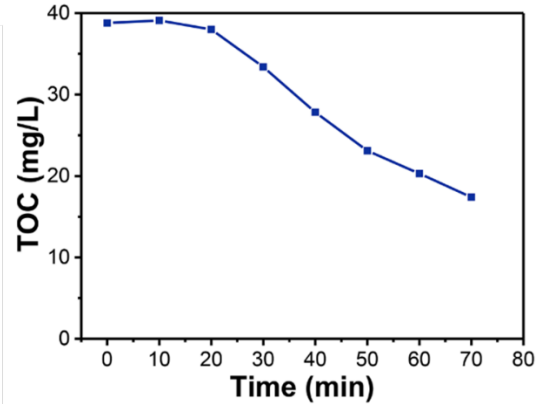

Fig. S11. Total organic carbon (TOC) variation in the phenol degradation process in this Fenton-like system. 50 ppm phenol + 500 ppm FeOCl-12h + 5.9 mg/L NaCl + 30 mM H_2O_2 (pH = 4, 4 mM HAc-NaAc buffer, 25 °C).

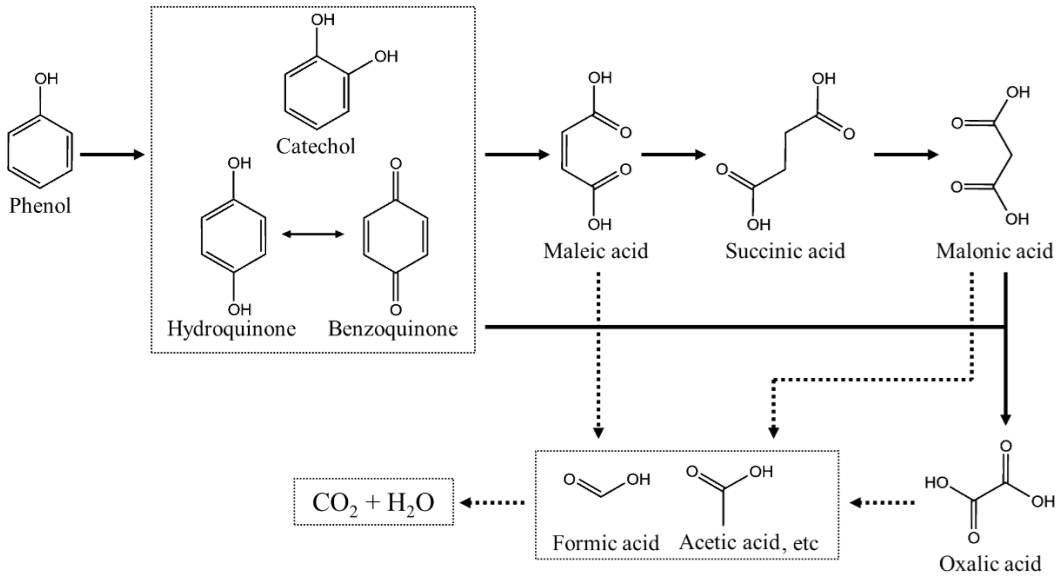

Fig. S12. The proposed reaction path of phenol degradation in this Fenton-like system.

10. Stability of FeOCl structure and properties

The cycling experiments and structural characterizations evaluated the stability of the fabricated FeOCl. After each round of experiments, the catalyst was separated by filtration using a 0.22 μm filter, washed with deionized water and acetone repeatedly three times, and placed in a vacuum oven at 40 °C for the next round of the experiment.

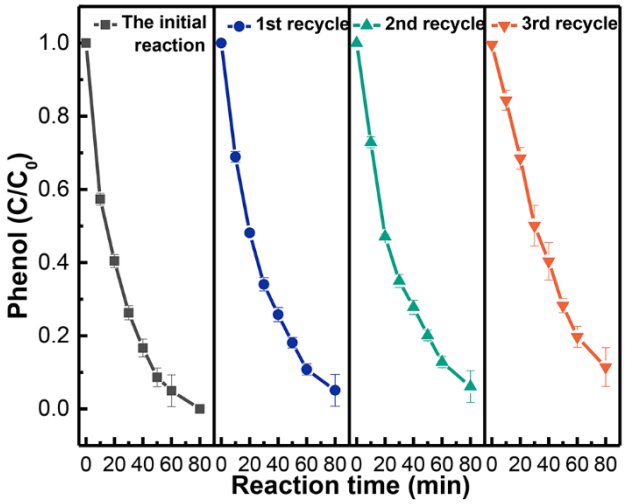

Fig. S13. Cycling experiment of the fabricated FeOCl. Reaction condition: 50 ppm phenol + 500 ppm FeOCl + 30 mM H_2O_2 (pH = 4, 4 mM HAc-NaAc buffer, 25 °C).

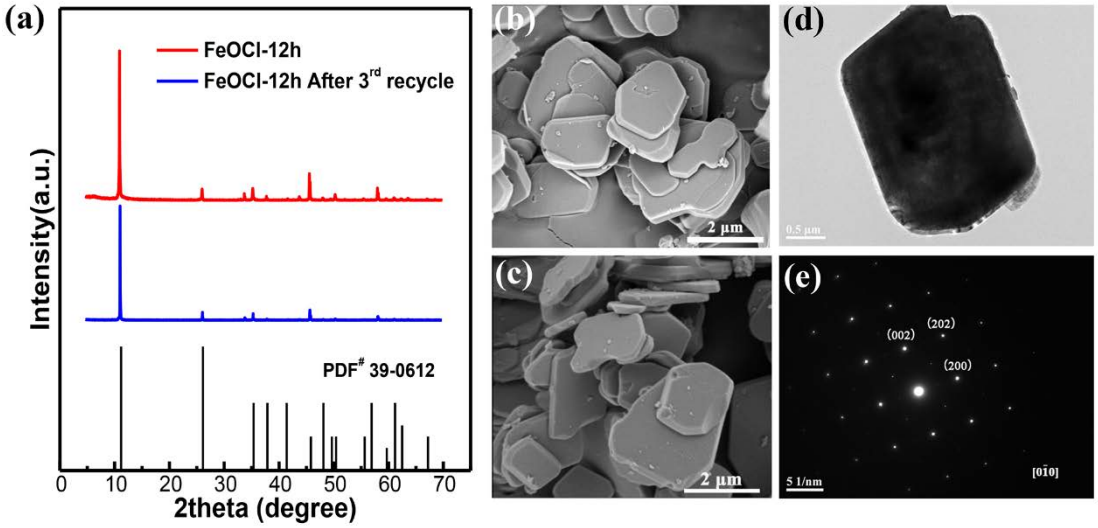

Fig. S14. (a)XRD pattern of FeOCl-12h before and after reaction; SEM images of FeOCl (b) before (c) the after the reaction; (d) TEM and (e) SAED of the reacted FeOCl.

Identical XRD peaks were observed after the reaction, consistent with the standard PDF card JCPDS No.39-0612 of FeOCl. Consistent results of SEM, TEM, and SAED characterization were also obtained, indicating the high robustness of the FeOCl catalyst during the reaction.

11. Different pH effects

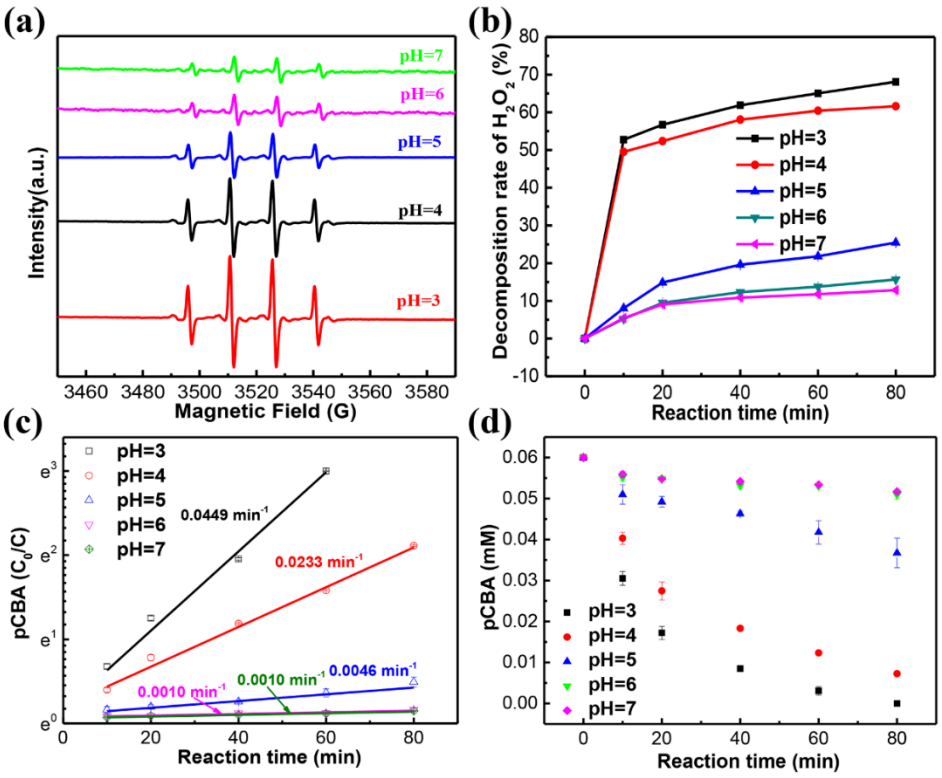

Fig. S15. (a) DMPO/OH· of FeOCl-12h in different pH solutions. (b) The decomposition of H_2O_2 in different pH solutions. (c, d) pCBA probe experiment of FeOCl-12h in different pH solutions. 180 mM DMPO; 30mM H_2O_2; 500 ppm FeOCl materials; 0.06 mM pCBA.

The results revealed that the fabricated FeOCl exhibited a higher capability of activating H_2O_2 and generating hydroxyl radicals under lower pHs with lower capability at higher pHs. Nevertheless, even under pH = 7, the regulated FeOCl could activate H_2O_2 to generate OH·, which was often not observed on Fe-based materials.

12. Comparison with other catalyst parameters

Table S6. Comparison study of phenol degradation in Fenton reaction using different catalysts

catalyst	pH	Initial conc (mg L^{-1})	Conc. of catalyst and H_2O_2	Removal of phenol and time	Leaching of Fe (mg L^{-1}) (ratio of Fe atoms%)	Ref.
Dendritic Fe^0	4	50	0.1g/L, 6mM	90%, 16min	2(2%)	[2]
	3.5	50	0.1g/L, 6mM	90%, 3min	8(8%)	
Fe_3O_4/MWCNTs	3	100	1g/L, 10mM	100%, 120min	2.5(1.38%)	[3]
FeOCl	4	100	0.2g/L, 15.6mM	100%, 30min	0.57-1.25(0.54-1.2%)	[4]
Fe_2O_3-ZrO_2	6	100	0.8g/L, 112mM(60°C)	100%, 210min	<0.5%	[5]
Schwertmannite	3	100	1g/L, 14.7mM	100%, 30min	5.0-27(0.92-4.95%)	[6]
	5	100	1g/L, 14.7mM	100%, 6h	2.5-13(0.46-2.47%)	
Fe-clay	3	50	1g/L, 7mM	100%, 7h	1.7(0.26%)	[7]
	4	50	0.5g/L, 10mM	100%, 10min	2.54(0.28%)	
Fe-Pd@C	5	50	0.5g/L, 10mM	99%, 60min	0.51(0.06%)	[8]
	6	50	0.5g/L, 10mM	95%, 60min	0.48(0.05%)	
FeOCl-12h	4	50	0.5g/L, 30mM	99%, 60min	0.47(0.04%)	this work

13. The effect of leached Fe and Cl

Table S7. The concentration of leaching Fe and Cl in the reaction solution.

After reaction		FeOCl-P	FeOCl-30nm	FeOCl-0.5h	FeOCl-2h	FeOCl-12h
Fe leaching	Concentration (mg/L)	0.29	0.37	0.40	0.44	0.47
	Proportion (%)	0.11	0.14	0.15	0.17	0.18
Cl leaching	Concentration (mg/L)	4.10	4.70	5.10	5.00	5.90
	Proportion (%)	2.48	2.85	3.09	3.03	3.57

We selected the largest leached iron concentration (0.47mg/L) to analyze the effect of leached iron on H_2O_2 activation. The formation of hydroxyl radicals (OH·) was measured using p-chlorobenzoic acid (pCBA) as a probe.

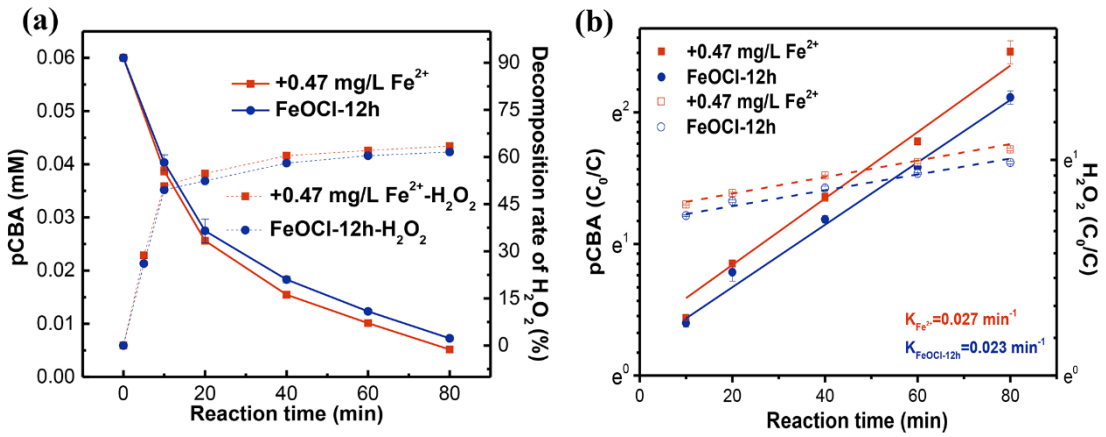

Fig. S16. Effect of leached iron on a system of H_2O_2 activation. Reaction condition: 0.06 mM pCBA + 500 ppm FeOCl + 0.47 mg/L Fe^{2+} + 30 mM H_2O_2 (pH = 4, 4 mM HAc-NaAc buffer, 25 ^oC).

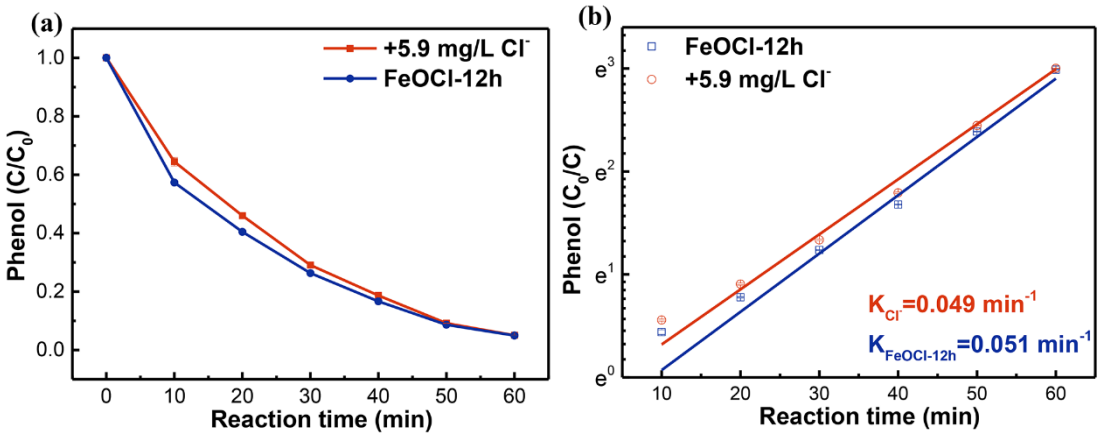

Fig. S17. Effect of leached Cl^- in the H_2O_2 activation system. Reaction condition: 50 ppm phenol + 500 ppm FeOCl + 5.9 mg/L NaCl + 30 mM H_2O_2 (pH = 4, 4 mM HAc-NaAc buffer, 25 °C).

REFERENCES

1. Wu C G, Degroot D C, Marcy H O, Schindler J L, Kannewurf C R, Bakas T, Papaefthymiou V, Hirpo W, Yesinowski J P. Reaction of aniline with FeOCl. Formation and ordering of conducting polyaniline in a crystalline layered host. Journal of the American Chemical Society, 1995, 117(36): 9229-9242
2. Xia Q X, Jiang Z H, Wang J K, Yao Z P. A facile preparation of hierarchical dendritic zero-valent iron for Fenton-like degradation of phenol. Catalysis Communications, 2017, 100: 57-61
3. Tian X J, Liu Y F, Chi W D, Wang Y, Yue X Z, Huang Q G, Yu C Y. Catalytic degradation of phenol and p-nitrophenol using Fe_3O_4/MWCNT nanocomposites as heterogeneous Fenton-like catalyst. Water, Air, & Soil Pollution, 2017, 228: 1-12
4. Yang X Y, Xu X M, Xu J, Han Y F. Iron oxychloride (FeOCl): An efficient Fenton-like catalyst for producing hydroxyl radicals in degradation of organic contaminants. Journal of the American Chemical Society, 2013, 135(43): 16058-16061
5. Gao P, Song Y, Hao M J, Zhu A N, Yang H W, Yang S X. An effective and magnetic Fe_2O_3-ZrO_2 catalyst for phenol degradation under neutral pH in the heterogeneous Fenton-like reaction. Separation and Purification Technology, 2018, 201: 238-243
6. Wang W, Song J, Han X. Schwertmannite as a new Fenton-like catalyst in the oxidation of phenol by H_2O_2. Journal of Hazardous Materials, 2013, 262: 412-419
7. Djeffal L, Abderrahmane S, Benzina M, Fourmentin M, Siffert S, Fourmentin S. Efficient degradation of phenol using natural clay as heterogeneous Fenton-like catalyst. Environmental Science and Pollution Research, 2014, 21: 3331-3338
8. He D W, Niu H Y, He S J, Mao L, Cai Y Q, Liang Y. Strengthened Fenton degradation of phenol catalyzed by core/shell Fe–Pd@C nanocomposites derived from mechanochemically synthesized Fe-Metal organic frameworks. Water research, 2019, 162: 151-160